# New Insight of Isothermal Melt Crystallization in Poly(aryl ether ether ketone) via Time-Resolved Simultaneous Small-Angle X-ray Scattering/Wide-Angle X-ray Diffraction Measurements

**Benjamin S. Hsiao,* Bryan B. Sauer, and Ravi K. Verma†**

*DuPont Central Research & Development, Experimental Station, Wilmington, Delaware 19880*

**H. Gerhard Zachmann and Sönke Seifert**

*Institut für Technische und Makromolekulare Chemie, Universität Hamburg, Hamburg, Germany*

**Benjamin Chu and Paul Harney**

*Department of Chemistry, State University of New York at Stony Brook, Stony Brook, New York 11794-3400*

*Received May 8, 1995; Revised Manuscript Received July 20, 1995®*

ABSTRACT: Isothermal melt crystallization (stage I, at 290 °C) and subsequent annealing (stage II, at about 287 °C) of poly(aryl ether ether ketone) was studied by time-resolved simultaneous small-angle X-ray scattering (SAXS) and wide-angle X-ray diffraction (WAXD) methods using synchrotron radiation. At stage I, both crystalline WAXD and SAXS peaks occurred almost simultaneously within the resolution time of our setup (30 s). WAXD profiles revealed a typical increase in the apparent crystallinity index and a slight rise in the crystal density with time, whereas SAXS profiles revealed decreases in both long period $L$ and lamellar thickness $l_C$ (estimated from the correlation function assuming a two-phase model) and a slight increase in the interlamellar noncrystalline layer thickness. At stage II, the annealing at a lower temperature caused anisotropic changes in the unit cell dimensions: $b$ (along the spherulitic growth direction) was found to remain about constant, while $a$ (perpendicular to the growth direction) decreases noticeably. Other induced variations include a subsequent increase in the crystallinity index and decreases in $L$, $l_C$, and invariant $Q$. These results are consistent with a proposed model comprising primary crystallization from the unrestrained melt which produces thicker lamellar stacks, and subsequent infilling secondary crystallization from the restrained melt which produces thinner lamellar stacks with smaller $L$ and $l_C$.

## Introduction

It has been established that more than 80% of crystalline polymers can melt crystallize into a lamellar morphology with long periods ranging from 100 to 1000 Å.[1,2] This morphology consists of alternating crystalline and amorphous phases in lamellar stacks, which are identifiable by transmission electron microscopy (TEM)[3] and small-angle X-ray scattering (SAXS).[4] However, the events and factors that result in the formation of such a morphology are not understood, largely due to the absence of suitable real-time characterization tools. In our laboratory (at DuPont), a simultaneous SAXS/wide-angle X-ray diffraction (WAXD) apparatus for synchrotron X-ray study was constructed for this purpose. This apparatus is capable of revealing both morphological and structural changes with a time resolution of a few seconds. Similar devices have also been constructed in several laboratories.[5,6] This paper summarizes some previously unreported findings during the isothermal crystallization and subsequent annealing at a slightly lower temperature in poly(aryl ether ether ketone) (PEEK). We are in the process of investigating other semicrystalline systems to confirm whether the observed behavior is truly universal.

Our first objective is to understand the morphological development during the initial stage of melt crystallization. This includes the induction period before primary crystallization. Our interest in the induction period is prompted by the recent finding of Kaji *et al.*,[7] who crystallized an amorphous poly(ethylene terephthalate) (PET) sample heated above its glass transition temperature. They observed large-scale density fluctuations (which manifest in SAXS) before any crystalline lattice like order (which manifest in WAXD). A similar finding has also been reported in poly(aryl ether ketone ketone) copolymers by Ezquerra *et al.* using synchrotron X-rays.[8] However, both experiments were performed during cold crystallization, and a similar behavior has not been demonstrated during melt crystallization. One indication for a likely behavior during melt crystallization comes from recent *on-line* synchrotron SAXS and WAXD studies during melt spinning of poly(vinylidene fluoride) fibers by Cakmak *et al.*[9] They observed that SAXS profiles always appeared before WAXD peaks along the spin line. However, it may be argued that the spinning process produces flow instability which leads to the initial density fluctuations. It is thus our goal to investigate this matter during isothermal melt crystallization from unoriented samples.

Our second objective is to understand the rather ill-defined stage of secondary crystallization. Secondary crystallization generally implies the stage that deviates from simple Avrami kinetics. Little is known about the morphological changes that take place during this stage

* To whom all correspondence should be addressed.
† Present address: Chemistry Department, Virginia Polytechnic Institute and State University, Blacksburg, VA 24061.
® Abstract published in *Advance ACS Abstracts,* September 1, 1995.

0024-9297/95/2228-6931$09.00/0 

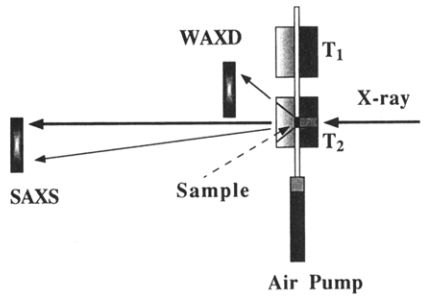


**Figure 1.** Diagram for a simultaneous SAXS/WAXD/dual-cell temperature jump unit setup.

in melt crystallization. Recently, there have been some suggestions that secondary crystallization takes place in "liquid pockets" under negative pressure.[10] The liquid pockets are the interfibrillar (or interlamellar stack) regions,[12] and the negative pressure is related to the internal stress which evolves due to local densification due to the higher density of the crystal.

The present study is part of a larger effort to understand the mechanism of primary and secondary crystallization. We intend to obtain some in-depth information about this stage by further imposing a sub-$T_c$ (by only a few degrees Celsius) annealing after isothermal crystallization. Detailed information about crystal unit cell parameters and the crystallinity index are to be extracted from the WAXD data, and morphological variables such as long period $L$, lamellar thickness $l_C$, and interlamellar noncrystalline thickness $l_A$ are to be estimated from the SAXS data. The chosen system is PEEK. It is selected because of its well established structural, morphological and thermal information.[11-15] Also it serves a good model for other systems. Future studies on other model systems such as PET, PE and nylon 66 are underway.

## Experimental Section

PEEK samples were purchased from ICI in the form of pellets (type 150G). Isothermal crystallization and subsequent annealing measurements were carried out in a dual-cell temperature jump unit.[15] The setup diagram is shown in Figure 1. The melt temperature ($T_1$) was maintained at 400 °C; the isothermal crystallization temperature ($T_2$) was set at 290 °C for about 1200 s (stage I) and then dropped to ca. 287 °C for subsequent annealing treatment (stage II). The accuracy of $T_2$ for stage I is within ±0.5 °C, and for stage II it is within ±1.5 °C. Some evidence of a drift in temperature on the order of 5 °C is observed in stage II. The time required to equilibrate at the crystallization temperature after the initial "jump" is less than 60 s. The sample was first held at 400 °C for 30 min. This relatively severe melting condition might result in some cross-linking or degradation, but it also slows down the crystallization kinetics. Slower crystallization kinetics enables us to study the melt crystallization at a low crystallization temperature (290 °C) with a relatively long data collection time (30 s).

The synchrotron experiment was carried out at the X3A2 Beamline (bending magnet line, $l$ = 1.5 Å) at the National Synchrotron Light Source (NSLS), Brookhaven National Laboratory, using modified Kratky optics (beam size 1.5 mm × 0.5 mm) and a sample to detector distance of 136 cm. Two linear position-sensitive detectors (Braun) controlled by separate multichannel analyzer interface boards (Nucleus PCA-II, Oxford, for SAXS; Maestro-II, EG&G, for WAXD) were used for the simultaneous SAXS/WAXD measurements. In this setup (Figure 1), the angular range ($2\theta$) for SAXS was from 2.4 to 36 mrad, and for WAXD it was from 14° to 28°. We found that the WAXD measurement time lagged behind about 1% of the collection time for SAXS measurement (for which time was used as the reference) due to the difference in the

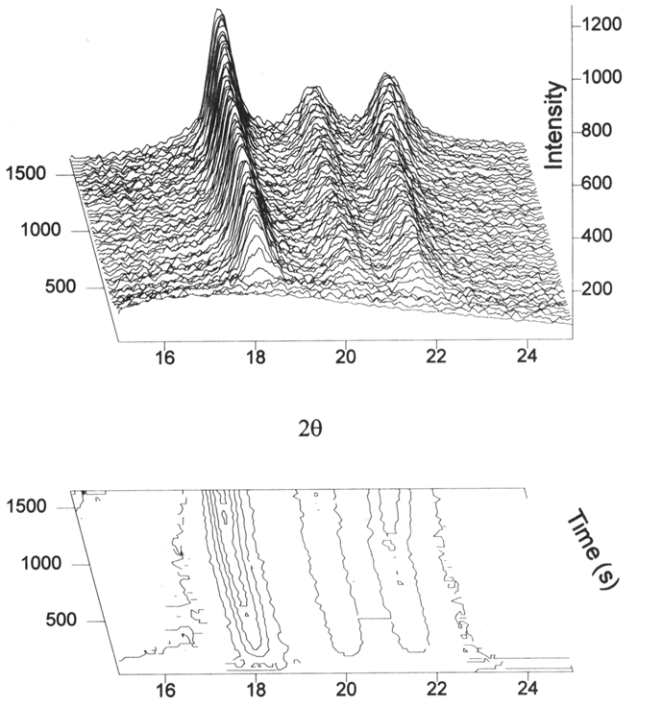


**Figure 2.** Excess crystalline WAXD profiles during isothermal crystallization (290 °C) and subsequent annealing (288 °C) measurement. The bottom diagram represents the isointensity contour plot projected from the top.

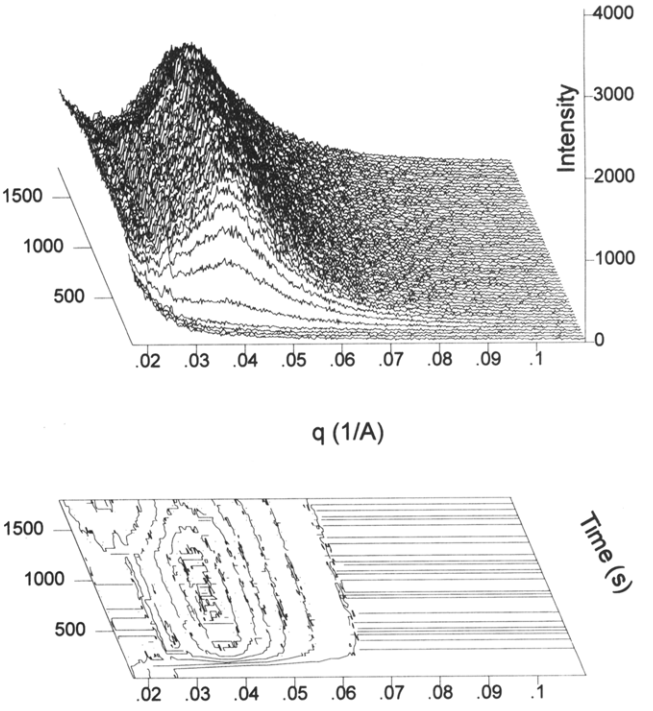


**Figure 3.** Corresponding SAXS profiles after the experimental and sample absorption corrections.

acquisition software. The time scale for different measurements was corrected accordingly. A vertical receiving slit (about 1 mm width) was adopted to enhance the angular resolution of WAXD signals from the slit optics.

## Results and Discussion

Time-resolved WAXD profiles of PEEK during this measurement are shown in Figure 2, and the corresponding SAXS profiles are shown in Figure 3. In both figures, the top diagram represents the 3D plot of diffraction or scattering patterns as a function of time,

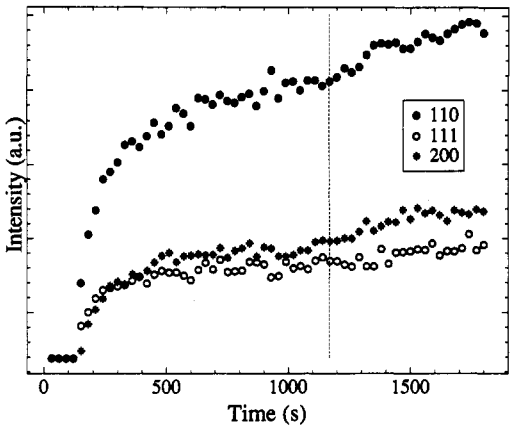


**Figure 4.** Integrated intensity as a function of time for each reflection from WAXD profiles.

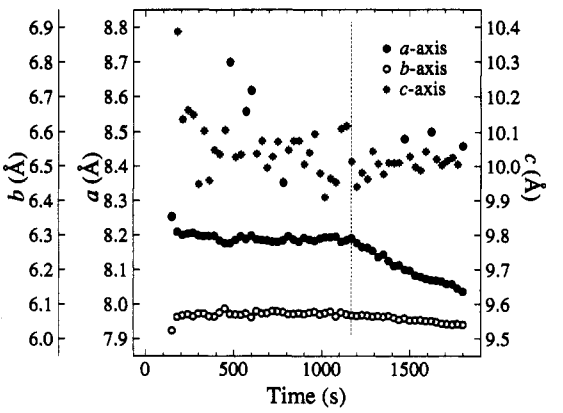


**Figure 5.** Crystal unit cell dimensions calculated from the peak positions from WAXD profiles.

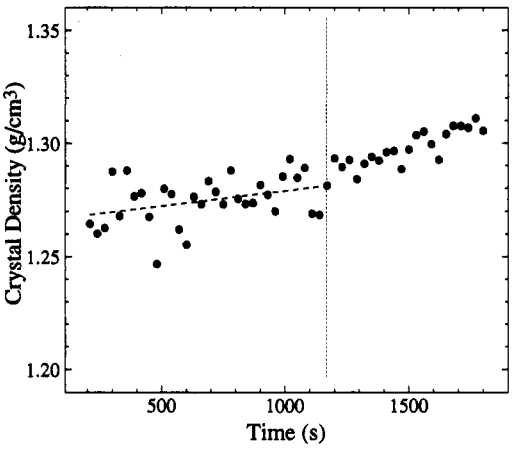


**Figure 6.** Corresponding crystalline density as a function of time from Figure 5.

and the bottom diagram represents the isointensity contour plot projected from the top. All profiles have been corrected for incident beam intensity fluctuations, attenuation within the sample, and parasitic scattering. Further, from the WAXD profiles the initial amorphous pattern in the melt was scaled and subtracted. Therefore, the WAXD profiles represent the excess intensity resulting from the crystalline phase. In these figures, it is seen that both WAXD and SAXS "crystal signature" profiles begin almost simultaneously at 150 s (the fifth curve). Note that WAXD detects the three-dimensional crystal structure and SAXS detects large-scale density fluctuations. In light of that, the above results suggest the following. If the density fluctuations truly occur as a precursors for crystallization from the melt (as suggested by the cold crystallization study[7,8]), then the time difference between the two mechanisms (fluctuation precursor and crystallization) may be smaller than the resolution time of our setup (30 s). Conversely, the volume fraction of fluctuation precursor material may be too small to detect by SAXS because of the low volume fraction of nuclei for the melt-crystallized system as opposed to the cold crystallization system.[7,8] This issue deserves further investigation with a higher flux synchrotron source (from an undulator or wiggler source) which would enable a much shorter collection time.[16]

From the WAXD profiles (Figure 2), several unique features were observed. At stage I (<1200 s, isothermal crystallization), the intensity of the three crystalline peaks (which can be indexed as 110, 111, and 200) increased with time, and the peak positions of the three reflections remained about constant as expected. However, upon the subsequent annealing at ca. 287 °C (>1200 s, stage II), the peak positions of both 110 and 200 were found to shift to higher angles. The integrated intensity of each reflection (after deconvolution) is illustrated in Figure 4. The dotted line indicates the beginning of the temperature reduction. It is likely that the temperature is never completely constant over the stage II region. The overall growth of the different reflections at stage II has the following order 110 ≫ 200 > 111. However, the 111 peak grows at a faster rate compared to the 200 peak during the initial stage of crystallization (I). While this difference might be due to some experimental artifact, it could also imply that some crystal perfection is taking place. From the sum of the three integrated intensities and the area of the scaled amorphous pattern, a crystallinity index can be estimated. Note that this index does not represent an absolute crystallinity but an estimate which should only be compared with itself. This crystallinity index increases with measurement time and does not equilibrate within our measurement period.

The unit cell dimensions of PEEK can be calculated from the $2\theta$ positions of the three reflections assuming a two-chain orthorhombic unit cell. The unit cell estimates are shown in Figure 5, where the same $y$-axial scale is used for easy comparison. As shown in the plot, both $a$ and $b$ have similar precision, but $c$ shows a larger uncertainty. This is expected since $c$ is estimated from the 111 reflection and requires the values of $a$ and $b$. Therefore, errors in $a$ and $b$ are added to the error in estimating the position of the 111 reflection, resulting in larger errors in $c$. At stage I, a very slight decrease in $a$ is observed and the overall changes in $a$ and $b$ are small. This is quite different from stage II, where $a$ *declines significantly with time* and $b$ remains almost constant. The crystalline density calculated from the unit cell parameters is shown in Figure 6. It is seen that the crystal density increases in both stages. Similar results have also been observed in PEEK,[17] PPS, and PET[17,18] that the crystalline density was found to increase with time during isothermal annealing. In those studies, the analysis was carried out from the WAXD data collected at room temperature on quenched samples after different annealing times at isothermal temperatures.

It has been demonstrated by Lovinger *et al.*[12] that, in PEEK, the $b$ axis represents the spherulitic growth direction, the $c$ axis represents the lamellar thickness direction, and $a$ is orthogonal to both $b$ and $c$. Since a considerable densification of the unit cell along the $a$

axis (orthogonal to both the lamellar thickness and the growth directions) at stage II was observed, we present two speculative models consistent with the above observation. (1) Viscoelastic relaxation of internal stress (tensile, on the crystal) continuously occurs at these very high temperatures. It is reasonable that the original stress due to the local densification during crystallization is directional and is normal to the growth direction. As this stress relaxes the strain on the crystal in the $a$ direction gives rise to the observed result. (2) The second model is related to the stress imposed upon the primary lamellae by secondary crystallization. The crystal/melt interfaces in the growth direction ($b$ axis) may be considered to be in a steady state during primary crystallization and probably independent of secondary crystallization. On the other hand, the crystal/melt interface orthogonal to the growth direction (along the $a$ and $c$ axes) must be sensitive to the occurrence of secondary crystallization in the neighboring liquid pocket. As a result, secondary crystallization may impose large elastic strains along the $a$ and $c$ axes of the primary lamellae but not along the $b$ axis, which leads to a larger decrease in $a$ than $b$ at stage II.

Any trends in the $c$ axis are probably hidden in the noise in its estimate. If we assume crystallization results in a negative pressure in the amorphous environment, the observed decrease in $a$ suggests that a "reduced" negative pressure (which leads to a decrease in internal stress) perhaps exists perpendicular to the growth direction. The relaxation of this negative pressure within the stacks probably also manifests in a relaxation of stress on the liquid pockets between primary lamellar stacks. Recently, there have been some arguments by Marand *et al.*[10] that secondary crystallization takes place within the liquid pockets which are under negative pressure. They argue that the low endotherm observed in semicrystalline systems such as PEEK is the result of this negative pressure exerted on the secondary lamellae. WAXD data suggest more directly the existence of a relaxation of this negative pressure with time. Further, our argument in favor of a relaxation of internal stress is supported by the analysis of SAXS data which is discussed subsequently. The issue is far from being clear and definitely deserves further investigation.

Morphological variables such as long period $L$ and thicknesses of both phases ($l_1$ and $l_2$; $l_1 > l_2$) can be extracted from the correlation function of SAXS data using the 2-phase model of Strobl and Schneider.[19] We have used a novel approach by adopting a modified form of Porod's law to calculate the correlation function. This method facilitates the correction of liquid scattering and crystal/melt interfacial thickness for the determination of the Porod constant.[20] The calculated time-resolved correlation functions are shown in Figure 7, and the extracted morphological variables are depicted in Figure 8. Care should be taken while using these extracted variables for any subsequent analysis. Preliminary modeling work in our group demonstrates[21] that the Strobl and Schneider approach of an ideal two-phase model results in erroneous estimates for $l_1$ and $l_2$ when applied on several nonideal two-phase models. However, given the absence of a better technique to estimate $l_1$ and $l_2$ (we were unable to estimate the interface distribution function for the current scattering data due to a limited angular range and a low signal-to-noise ratio at high $q$), we have used the ideal two-phase model to extract $l_1$ and $l_2$ from the correlation function. We

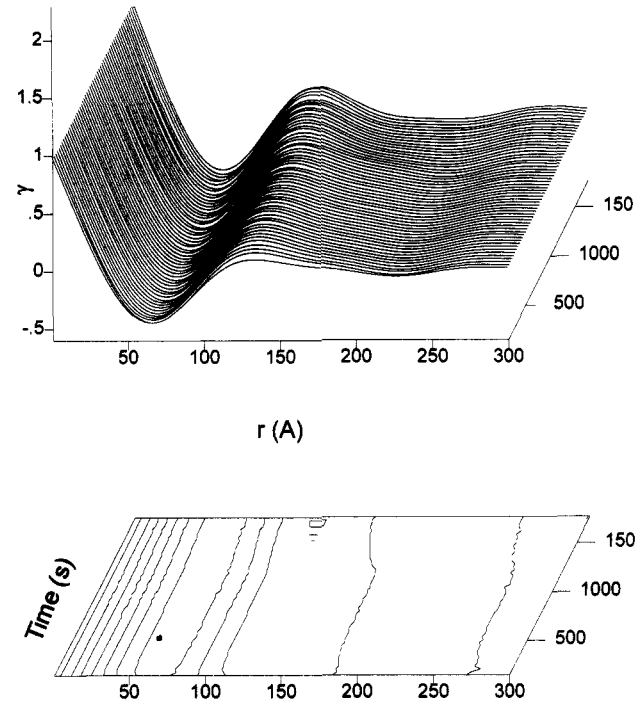


**Figure 7.** Correlation functions calculated from the time-resolved SAXS profiles.

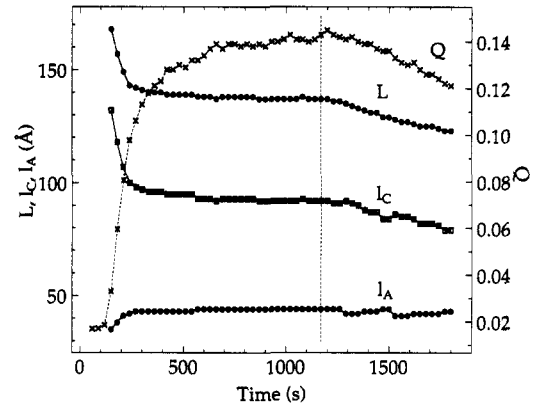


**Figure 8.** Estimated values of long period $L$, lamellar thickness ($l_C$), interlamellar noncrystalline layer thickness ($l_a$) and invariant $Q$ as functions of time from Figure 7. The change in slope at $t$ = 1170 s is in part due to a slow decrease in temperature over this period.

acknowledge the fact that this approach will result in some error; however, the trends in $l_1$ and $l_2$ remain almost unaffected as indicated by our modeling work.[21]

From the correlation function alone, one cannot assign the two calculated thicknesses $l_1$ and $l_2$ to the crystalline and interlamellar noncrystalline layer thicknesses. However, in this work, we have assigned the larger $l_1$ to the lamellar thickness and $l_2$ to the interlamellar noncrystalline thickness (some authors make the assignment inversely[22]). The reasons for our assignment are as follows. (1) We have found that room temperature WAXD crystallinity in PEEK samples with similar thermal histories is typically greater than 20% and can be as high as 40%.[23] On the other hand, the linear fraction of the smaller phase never exceeds 35% at high temperature (this work and previous data[15]) and can be as low as 25% at room temperature.[15,24] Thus, the larger $l_1$ must be crystalline and the smaller $l_2$ must be the noncrystalline layer, otherwise, the criterion of mass balance for the crystalline phase cannot be met. (2) TEM micrographs from thin films and from etched

replicated surfaces suggest that the average lamellar thickness is about 80 Å.[11,12] (3) Some unpublished SAXS data[21] indicate that smaller $l_2$ increases with temperature even below the glass transition temperature (the larger $l_1$ remaining about constant). Since the average lamellar thickness is not expected to change below the glass transition temperature, the smaller $l_2$ must necessarily be assigned to the noncrystalline layer thickness. (4) A line-width analysis[25] of the WAXD peaks for a lower limit for crystal thickness along the $c$ axis yields a value of about 60 Å, which is consistent only with our assignment. (5) We believe that the existence of crystalline lamellae with a thickness of about 20 Å (about two repeat units) would be physically unreasonable. Such a value in $l_2$ is often observed at the initial crystallization stage under a large supercooling.[15] (6) Finally, TEM clearly shows that the lamellar stacks are not spaced filling;[12] i.e., there are broad gaps between the crystalline fibrils. Thus, the linear crystallinity (determined to be 70% if $l_1$ is lamellar thickness) cannot be equal to be bulk crystallinity (i.e., 35%), proving that $l_2$ is not the lamellar thickness.

Returning to the SAXS-extracted parameters, we first discuss the results for stage I crystallization between 50 and 1200 s. The lamellar thickness $l_C$ decreases with time, whereas the noncrystalline layer thickness $l_A$ increases slightly with time in the region where $Q$ is increasing sharply (Figure 8). As $Q$ begins to level out at about 400 s, the spherulites are space filling under these conditions. The relatively large decrease in long spacing and lamellar thickness during the initial stage of crystallization (between 150 and 220 s in Figure 8) has been observed previously.[15] In earlier work,[6,15] it had been suggested that this initial decrease might be due to the insertion of additional lamellae within a primary lamellar stack. Indirect evidence against this insertion mechanism is seen in results suggesting that the interlamellar noncrystalline regions are entirely "rigid"[26] and extremely narrow (on the order of 50 Å or less,[15,26] see also in Figure 8). It is more likely that this sharp initial decrease is reflective of secondary crystallization producing thin lamellar stacks within the liquid pockets.[10] The SAXS method projects the bulk lamellar morphology therefore cannot distinguish the two mechanisms easily by itself.

The argument of thinner lamellae being produced by secondary crystallization can also be explained by a thermodynamic standpoint. If secondary crystallization undergoes a relaxation of negative pressure (or internal stress) as discussed earlier, the increased pressure will undoubtedly raise the equilibrium melting temperature, thereby reducing the critical lamellar thickness required for the formation of a stable nucleus. In other words, thinner lamellae can be stabilized within the liquid pocket where the melt is restrained. In light of this, we would like to emphasize that, *during isothermal condition, primary crystallization always takes place from the "equilibrium" melt and produces thicker lamellae, whereas secondary crystallization takes place from the melt restrained by the primary crystals and produces thinner lamellae.* It is apparent that secondary crystallization is an in-filling process, which must be considered at any crystallization stage whenever the state of the crystallizable melt starts to deviate from the virgin melt.

The slowdown in the changes in the morphological variables at the later part of stage I (between 250 and 1200 s in Figure 8) is consistent with the very slow secondary crystallization process. The contribution of the secondary lamellae which form slowly, when averaged with the signal from the dominant primary lamellae, gives rise the observed slow decrease in $L$ and $l_C$, and very small increase in $l_A$. This is in contrast with the relatively large change in $L$ and $l_C$ at the initial crystallization stage when the population of primary lamellae are not dominant. The viscoelastic relaxations and internal stress in the liquid pockets should vary significantly because of the wide range of sizes of the liquid pockets. This would also explain part of the slowdown in the secondary processes.

In stage II after 1200 s, the temperature is dropped about 5 °C, leading to a decrease in the slope of $Q$, $L$, and $l_C$ (Figure 8). The drop in both $L$ and $l_C$ is consistent with the formation of new thinner lamellae by increasing the degree of supercooling. However, the decrease in $Q$ reflects a different mechanism. It is probably due to the decrease in density contrast between the crystal and amorphous phases rather than the change in morphology. This phenomenon has been observed in the reversed experiment. It is found that, during heating, $Q$ always increases with temperature as a result of different thermal expansion coefficiencies between the two phases, leading to an increasing scattering contrast for SAXS.[6,15]

## Conclusion

Simultaneous SAXS and WAXD measurements were carried out during isothermal crystallization and subsequent annealing on a PEEK sample. During the isothermal crystallization process (stage I), both crystalline WAXD and SAXS peaks were found to occur almost simultaneously within the resolution time of our setup (30 s). The WAXD data were analyzed for a crystallinity index and for the unit cell dimensions. The SAXS data were analyzed for the long period $L$, lamellar thickness $l_C$, noncrystalline layer thicknesses $l_A$ and invariant $Q$. We found the trends in the morphological variables and in the unit cell parameters during the stage II annealing indicate the existence of relaxation of internal stress (negative pressure) during crystallization. The evidences include decreases in the crystallographic $a$ axis, long period, and lamellar thickness and a slight increase in the interlamellar noncrystalline layer thickness at the initial stage. In addition, we observed that the crystallographic $b$ axis along the spherulitic growth direction is relatively insensitive to the variation of time and temperature. We have proposed different mechanisms for anisotropic variations in cell dimensions, and acknowledge the possible existence of others that we might have overlooked. Finally, we feel the melt crystallization model consisting of the steady-state primary process in the unrestrained melt (which produces thicker lamellar stacks) and the subsequent infilling secondary process in the restrained melt (which produces thinner lamellar stacks) is most consistent with our results.

**Acknowledgment.** The authors thank Dr. Herve Marand of Virginia Polytechnic Institute and State University and Dr. Stephen Z. D. Cheng of University of Akron for very helpful discussions and Mr. J. P. McKeown for assistance with synchrotron measurements. B.C. gratefully acknowledges support of this research by the National Science Foundation, Polymers Program (DMR9301294).

## References and Notes

(1) Wunderlich, B. *Macromolecular Physics*; Academic Press: New York, 1976; Vols. 1–3.

(2) Bassett, D. C. *Principles of Polymer Morphology*, Cambridge Press: Cambridge, U.K., 1981.
(3) Woodward, A. E. *Atlas of Polymer Morphology*, Hanser: New York, 1988.
(4) Glatter, O.; Kratky, O. *Small Angle X-ray Scattering*; Academic Press: New York, 1982.
(5) Bras, W.; Derbyshire, G. E.; Ryne, A. J.; Mant, G. R.; Felton, A.; Lewis, R. A.; Hall, C. J.; Greaves, G. N. *Nucl. Instrum. Methods Phys. Res.* **1993**, *A326*, 587
(6) Krüger, K. N.; Zachmann H. G. *Macromolecules* **1993**, *26*, 5205.
(7) Imai, M.; Mori, K.; Mizukami, T.; Kaji, K.; Kanaya, T. *Polymer* **1992**, *33* (21), 4451, 4457.
(8) Ezquerra, T. A.; López-Cabarcos, E.; Hsiao, B. S.; Baltà-Calleja, F. J. *Phys. Rev. Lett.*, submitted for publication.
(9) Cakmak, M.; Teitge, A.; Zachmann, H.; White, J. *J. Polym. Sci., Polym. Phys.* **1993**, *31*, 371.
(10) Marand, H.; Velikov, V.; Verma, R. K.; Cham, P. M.; Prabhu, V.; Dillard, D. *Polym. Prepr. (Am. Chem. Soc., Div. Polym. Chem.)* **1995**, *36* (1), 263.
(11) Blundell, D. J.; Osborn, B. N. *Polymer* **1983**, *24*, 953.
(12) Lovinger, A. J.; Davis, D. D. *J. Appl. Phys.* **1985**, *58* (8), 2843; *Macromolecules* **1986**, *19*, 1861.
(13) Bassett, D. C.; Olley, R. H.; Al Raheil, I. A. M. *Polymer* **1988**, *29*, 1945.
(14) Cheng, S. Z. D.; Cao, M. Y.; Wunderlich, B. *Macromolecules* **1986**, *19*, 1868.
(15) Hsiao, B. S.; Gardner, K. H.; Wu, D. Q.; Chu, B. *Polymer* **1993**, *34*, 3986, 3996.
(16) The current study was carried out in a bending magnet synchrotron source which produces about $10^{11}$ photons/s. The typical collection time has to be around seconds to obtain a 12-bit dynamic range (maximum signal/noise). It is possible to conduct a similar measurement in an undulator synchrotron source which produces $10^{12}-10^{13}$ photons/s with 1−2 orders of magnitude reduction in collection time.
(17) Chung, J. S.; Bodziuh, J.; Cebe, P. *J. Mater. Sci.* **1992**, *27* (20), 5609.
(18) Zhang, A.; Jiang, H.; Wu, C.; Qian, B. *J. Appl. Polym. Sci.* **1991**, *42(6)*, 1779
(19) Strobl, G. R. and Schneider, M. J. *J. Polym. Sci., Part B: Polym. Phys.* **1981**, *18*, 1355.
(20) Verma, R.; Biswas, A.; Hsiao, B. S. *J. Appl. Crystallogr.*, submitted for publication.
(21) Verma, R.; Biswas, A.; Hsiao, B. S.; Marand, H. *J. Appl. Crystallogr.*, submitted for publication.
(22) Jonas, A.; Russell, T. P.; Yoon, D. Y. *J. Polym. Sci., Polym. Phys.*, in press.
(23) Verma, R. K.; Velikov, V., Srinivas, S., Wilkes, G. L. and Marand. H. *Polymer*, in preparation. The WAXD crystallinity was evaluated using the method of Hermans and Weidinger and also the Ruland method. A series of PEEK samples with different thermal histories were used. The crystallinity at room temperature was found to vary between 20 and 35% depending on the thermal history.
(24) Verma, R.; Hsiao, B. S.; Marand, H. *Macromolecules*, in preparation. A PEEK sample crystallized at 300 °C for 1 h was cooled to room temperature and heated at 2.5 °C/min. The SAXS data were analyzed in a similar fashion. Significant increases were observed in the smaller $l_2$ even below the glass transition temperature. No changes were observed in the larger $l_1$ below the glass transition temperature. The linear crystallinity at 100 °C is about 74%.
(25) Line-width analysis was performed on WAXD data collected on a PEEK sample crystallized at 300 °C. No correction for instrumental broadening was performed. The dimension along the $c$ axis was estimated from the ⟨111⟩ peak width using the Scherrer formula, simple geometric considerations, and values for the crystal size along the $a$ and $b$ axes from the ⟨110⟩ and ⟨200⟩ peak widths.
(26) Sauer, B. B.; Hsiao, B. S. *ACS Prepr., Polym. Mater. Sci. Eng.* **1993**, *69*, 35.

MA950606L